Journal Name

ARTICLE

Fast Electrosynthesis of Fe-Containing Layered Double Hydroxides Arrays toward Highly Efficient Electrocatalytic Oxidation Reactions †

Zhenhua Li,[a] Mingfei Shao,*[a] Hongli An,[a] Zixuan Wang,[a] Simin Xu,[a] Min Wei,*[a] David G. Evans[a] and Xue Duan[a]

A new electrochemical synthesis route was developed for the fabrication of Fe-containing layered double hydroxides (MFe-LDHs, M= Ni, Co and Li) hierarchical nanoarrays, which exhibit highly-efficient electrocatalytic performances toward several small molecules oxidation reactions (water, hydrazine, methanol and ethanol). Ultrathin MFe-LDH nanoplatelets (200-300 nm in lateral length; 8-12 nm in thickness) perpendicular to the substrate surface are directly prepared within hundreds of seconds (<300 s) under cathodic potential. The as-obtained NiFe-LDH nanoplatelet arrays display promising behavior in oxygen evolution reaction (OER), giving rise to a rather low overpotential (0.224 V) at 10.0 mA cm^{-2} with largely enhanced stability, much superior to previously reported electrooxidation catalysts as well as the state-of-art Ir/C catalyst. Furthermore, the MFe-LDHs nanoplatelet arrays can also efficiently catalyze several other fuel molecules oxidation (e.g., hydrazine, methanol and ethanol), delivering a satisfactory electrocatalytic activity and high operation stability. In particular, this preparation method of Fe-containing LDHs is amenable to fast, effective and large-scale production, which shows promising applications in water splitting, fuel cells and other clean energy devices.

Introduction

Small molecules electro-oxidation reactions (e.g., water, hydrazine, methanol or ethanol), as core processes of water splitting devices, metal-air batteries or fuel cells, have attracted considerable attention owing to the increasing demands for the renewable energy resources.[1-8] In practice, however, the anodic electro-oxidation processes are greatly constrained by high kinetic barrier (high overpotentials), sluggish reaction dynamics and instability of electrode materials. For instance, even with the presence of state-of-the-art precious catalysts (such as Pt,[9,10] Pd,[11-13] IrO$_2$[14] and RuO$_2$[15]), a substantial overpotential is still required to drive the oxidation of small molecules, such as hydrazine, ethanol and water. Moreover, noble catalysts also suffer from their scarcity, high cost and easy toxication. Recently, great efforts have been focused on the oxides/ hydroxides of first-row transition metals as promising electro-oxidation catalysts. Among them, cobalt-based composites,[16-19] perovskite oxides[20-22] and oxyhydroxides (e.g., amorphous FeOOH and NiOOH)[23-25] were extensively studied and have shown interesting catalytic behavior. Despite all these progresses, the development of stable, efficient and cost-

effective electro-oxidation catalysts toward small molecules still remains a challenge.

Layered double hydroxides (LDHs) are a large class of typical inorganic layered materials which can be described by the general formula $[M^{II}_{1-x}M^{III}_x(OH)_2]^{z+}(A^{n-})_{z/n}$ yH$_2$O (M^{II} and M^{III} are divalent and trivalent metals respectively; A^{n-} is the interlayer anion compensating for the positive charge of the brucite-like layers).[26-31] Recently, LDHs materials have been found to show surprising oxygen evolution reaction (OER) performance and gained intensive attention as water oxidation catalysts.[32-45] For instance, Gong and coworkers reported that NiFe-LDH shows high electrocatalytic activity and stability for OER in alkaline environments than commercial precious metal-based catalysts.[36] Subsequently, various nanostructures of NiFe-LDHs (e.g., 2D single-layer nanoplatelets[37] and 3D architectural films[38]) as well as their nanocomposites (e.g., NiFe-LDHs/grapheme,[39-42] and NiFe-LDHs/carbon quantum dot[43]) with excellent OER performance have been further studied. Although these results indicate that NiFe-LDHs materials serve as rather good OER catalysts, the time- and cost-effective synthesis methods with good control over hierarchical nanostructures are highly necessary for further exploration of LDHs-based electrodes with enhanced properties. In addition, the generalized electrocatalytic oxidation properties of Fe-containing LDHs toward other small fuel molecules (e.g., hydrazine, methanol and ethanol) remain unknown. In the past decades, some advances have been made to find facile ways to prepare LDH materials (e.g., electrosynthesis method), with the

[a.] State Key Laboratory of Chemical Resource Engineering, Beijing University of Chemical Technology, Beijing 100029, China. E-mail: shaomf@mail.buct.edu.cn (M. Shao); weimin@mail.buct.edu.cn (M. Wei); Fax: 86-10-64425358; Tel: 86-10-64412131.

merits of fast and one-pot synthesis on electrode surface.[46-48] However, the development of fast and generally applicable methods for Fe-containing LDHs, so as to achieve excellent electrocatalysts toward small molecules oxidation reactions, is still a challenge in both scientific and technological condiserations.

Herein, we demonstrate the electrochemical approach as a fast, precisely controllable and economic method to fabricate various Fe-containing LDHs hierarchical nanoarrays for efficient electrocatalytic oxidation reactions. The homogeneous and uniform LDH nanoplatelets anchoring onto the surface of conducting substrates can be accomplished at room temperature within hundreds of seconds. Remarkably, the NiFe-LDH nanoplatelet arrays exhibits the optimal activity and long-term durability for water oxidation, in comparison with other electrocatalyst materials reported to date. Moreover, the electrocatalysis universality of NiFe-LDH arrays toward other small molecules oxidations in fuel cells (N_2H_4, CH_3OH and C_2H_5OH) has also been demonstrated. This time- and cost-effective synthesis route holds a great promise for the large-scale industrial manufacture, which is expected to show promising applications in renewable energy resources.

Results and Discussion

Structural and Morphological Characterization of MFe-LDH

Hierarchical MFe-LDH (M= Ni, Co and Li) nanoplatelet arrays are synthesized on the surface of foam nickel substrate via an electrosynthesis procedure followed by a self-oxidation process in air (Fig. 1a). The electrochemical synthesis was achieved by the following proposed reduction reaction on the working electrode: $NO_3^- + H_2O + 2e^- \rightarrow NO_2^- + 2OH^-$, in which the resulting OH^- leads to the precipitation of $M_xFe_{1-x}(OH)_2$. The whole electrosynthesis process is finished successively within hundreds of seconds at the room temperature. The as-synthesized $M_xFe_{1-x}(OH)_2$ material presents a light green color (Fig. 1b); After exposure in air for ~1 h, the sample color changes from green to a brownish one, indicating the occurrence of self-oxidation of Fe^{2+} to Fe^{3+}. Since it is hard to collect the MFe-LDH (M= Ni, Co and Li) powdered sample from the Ni foam to measure their XRD patterns, Fig. 1c illustrates the XRD patterns of MFe-LDH (M= Ni, Co and Li) samples via electrosynthesis on Ni foil substrate. The clear reflections of (003), (006) and (009) are observed for all these three MFe-LDH samples, which can be assigned to a typical LDH phase. The FT-IR technique was also used to identify the nature and symmetry of interlayer anions of MFe-LDHs (Fig. S1). The spectra of all the three samples show broad intense bands between 3600 and 3200 cm^{-1} due to the OH stretching mode of hydroxyl groups in host layers and interlayer water molecules. The band at 1507 cm^{-1} with its accompanying band at 1359 cm^{-1} is attributed to mode v3 of interlayer carbonate species. Surface elemental analysis was carried out by XPS over the MFe-LDH (M= Ni, Co and Li) nanoplatelet arrays. The full XPS spectra of MFe-LDH (Fig. 1d) show peaks located at 856.0 eV (NiFe-LDH), 780.9 eV (CoFe-LDH) and 55.8 eV (LiFe-LDH), corresponding to the 2p levels of Ni^{2+},
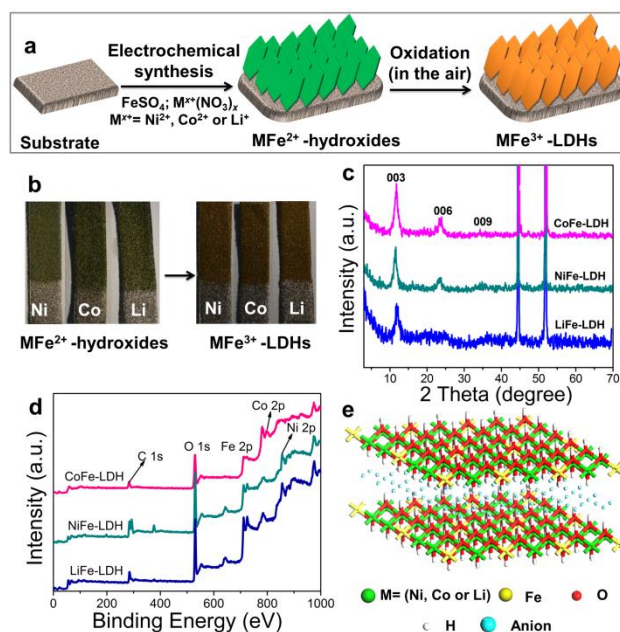

Fig. 1 (a) Scheme of the synthetic route to MFe-LDH (M= Co, Ni and Li) nanoarrays; (b) photograph of MFe-LDH nanoarrays growing on the Ni foam before and after self-oxidation in the air; (c) XRD patterns and (d) XPS spectra of MFe-LDH (M= Ni, Co and Li) nanoplatelet arrays; (e) structure model of MFe-LDH.

Co^{2+} and 1s of Li^+, respectively. The Fe $2p_{3/2}$ and Fe $2p_{1/2}$ spin-orbital splitting photo-electrons for all the three MFe-LDH samples are located at 711.0 and 724.9 eV, respectively (Fig. S2a), indicating the Fe (III) oxidation state in MFe-LDH (M= Ni, Co and Li) nanoplatelet arrays.[34] As shown in the XPS spectra of $NiFe^{2+}$ hydroxide and $NiFe^{3+}$-LDH sample (Fig. S2b), the binding energy of Fe 2p increases from 710.0 eV to 711.0 eV, further indicating the occurrence of self-oxidation of Fe^{2+} to Fe^{3+}.[49] Based on the results above, the crystal structure of the obtained LDHs is shown in Fig. 1e. Fig. 2a, 2b and 2c display typical SEM images of NiFe-LDH, CoFe-LDH and LiFe-LDH nanoplatelet arrays, respectively. Ultrathin and uniform NiFe-LDH platelets growing perpendicularly to the surface of substrate are observed, with 250–300 nm in lateral length and ~8 nm in thickness (Fig. 2a). By tuning the divalent metal precursor, CoFe-LDH (Fig. 2b) and LiFe-LDH (Fig. 2c) nanoplatelet arrays are also obtained with a similar plate-like microcrystal morphology and orientation, with narrow particle size distribution (CoFe-LDH: ~310 nm in lateral length and ~8 nm in thickness; LiFe-LDH: ~200 nm in lateral length and ~12 nm in thickness). In addition, the low magnification SEM images (Fig. S3a, 3c and 3e) for the MFe-LDH nanoplatelet arrays further verify the feasibility of the electrosynthesis method demonstrated here. Typical TEM images in Fig. 2d, 2e and 2f show individual nanoplatelet of NiFe-LDH, CoFe-LDH and LiFe-LDH, respectively. It is worth mention that the particle size of MFe-LDH (M= Ni, Co and Li) calculated by using Scherrer formula (50–80 nm) is apparently smaller than that of determined by SEM and TEM (200–300 nm), probably due to the presence of some amorphous LDHs phase. HRTEM image of the NiFe-LDH nanoplatelet (Fig. 2g) demonstrates a good crystallinity of the material. Interplanar distance of
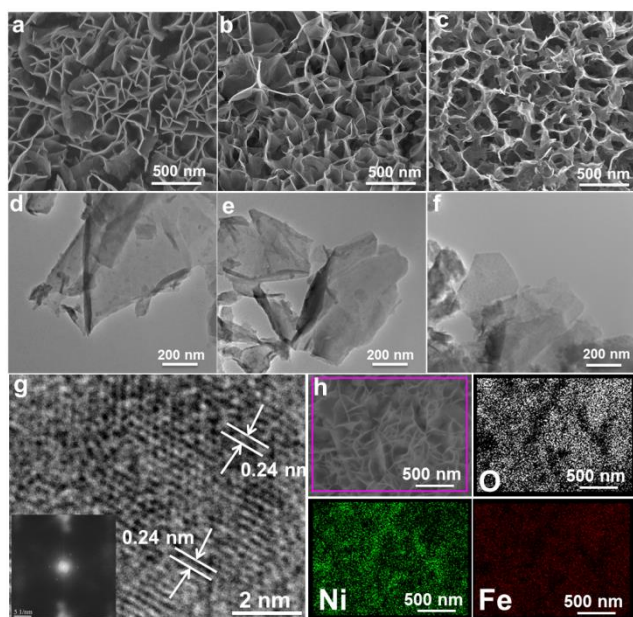
Fig. 2 SEM and TEM images of (a, d) NiFe-LDH, (b, e) CoFe-LDH and (c, f) LiFe-LDH nanoplatelet arrays; (g) HRTEM and (h) EDS mapping images for the NiFe-LDH nanoplatelet arrays.

0.24 nm is measured for a single-crystal particle, corresponding to the (012) plane of NiFe-LDH phase. The chemical compositions of as-obtained LDH nanoplatelet arrays are further determined by EDX technique. Figure 2h shows the EDX mapping analysis of NiFe-LDH, from which the iron and nickel are both homogeneously distributed on the surface of sample. The EDX spectra of MFe-LDH (M= Co, Ni and Li) nanoplatelet arrays (Fig. S3) also display the presence of M (Ni and Co; Li cannot be defined by EDX technique) and Fe, which is consistent with the mapping results. In addition, the M/Fe ratios of the three samples were further studied by using elemental analysis method (inductively coupled plasma-atomic emission spectroscopy, ICP-AES), and the obtained data are listed in Table S1. It is found that the three samples show rather close M/Fe molar ratios: 1.91, 1.89 and 1.85 for NiFe-, CoFe- and LiFe-LDH respectively, approximately consistent with the results of EDS analysis.

The formation process of such interesting MFe-LDH nanoplatelet arrays was further studied by control of the reaction time. Fig. S4 shows the SEM images of nine NiFe-LDH samples obtained with different electrosynthesis durations from 5 s to 500 s. A thin layer of nanoflake-like subunits appears on the surface of foam nickel with a short deposition time (5 s, Fig. S4a); numerous nanoflakes come into formation with the deposition time of 50 s (Fig. S4d). As the reaction time is further prolonged, the LDH nanoflakes with well-defined plate-like morphology grow much bigger and more densely with decreasing interspace. After 300 s of electrodeposition, the whole surface of foam nickel is covered with LDH nanoflakes uniformly (Fig. S4g), and a much denser LDHs modified surface is obtained with further longer synthesis time (Fig. S4h-i). Moreover, NiFe-LDH nanoplatelet arrays obtained with different electrochemical potentials (Fig. S5) and various

precursor concentrations (Fig. S6) were studied. The optimal synthesis condition for the NiFe-LDH arrays can be determined with the potential of −1.0 V *vs*. SCE in an electrolyte containing 0.15 M $Ni(NO_3)_2 \cdot 6H_2O$ and 0.15 M $Fe(SO_4)_2 \cdot 7H_2O$, which gives a good LDH crystalline and ordered array morphology.

Oxygen Evolution Reaction (OER)

The OER activity of MFe-LDH (M= Ni, Co and Li) nanoplatelet arrays and the reference sample (Ir/C) in alkaline solutions was evaluated in 1 M KOH using a standard three-electrode system. The mass-loading of Ir/C catalyst supported on Ni foam was controlled as the same value of MFe-LDH (M= Ni, Co and Li) samples (1 mg cm^{-2}), to give a reasonable comparison. Fig. 3a shows the polarization curves at a slow scan rate of 10 mV s^{-1} to minimize the capacitive current. The NiFe-LDH nanoplatelet array displays the lowest onset potential of OER current and the highest current density at the same overpotential (η) among these four electrocatalysts, revealing the highest electrochemical activity. Overpotentials at current density of 10 and 100 mA cm^{-2} for various catalysts are given in Fig. 3b. At 10 mA cm^{-2}, the as-prepared NiFe-LDH requires an overpotential of 224 mV, which is 64, 53, and 65 mV less than CoFe-LDH, LiFe-LDH and commercial Ir/C, respectively. Similarly, the overpotential of NiFe-LDH is also the lowest even at a high current density (100 mA cm^{-2}). The current density at η= 300 mV is 44.3 mA cm^{-2} for NiFe-LDH, which is ~3.1, 2.6 and 3.6 times of the current density for CoFe-LDH, LiFe-LDH and commercial Ir/C, respectively. The Tafel slope of NiFe-LDH is 52.8 mV dec^{-1} (Fig. 3c), much smaller than that of CoFe-LDH (92.0 mV dec^{-1}), LiFe-LDH (104.0 mV dec^{-1}) and Ir/C (145.0 mV dec^{-1}), indicating a superior OER performance of NiFe-LDH. The activity of MFe-LDHs nanoplatelet arrays was further investigated in apparent turnover frequencies (TOFs) (see Supporting Information for calculation details). The NiFe-, CoFe-, LiFe-LDH and Ir/C give TOF values of 0.013, 0.0075, 0.0054 and 0.0036 s^{-1} at η= 300 mV (Table S2), respectively, which implies the highest activity of NiFe-LDH nanoplatelet arrays. The actual oxygen production catalyzed by NiFe-LDH at a constant current of 100 mA cm^{-2} was obtained by using the water displacement method in an air-tight reactor to measure the Faradaic yield for O_2 formation (Fig. S7). The catalyst shows a Faradaic efficiency of 99.4% after an induction period of 10 min, indicating a satisfactory energy conversion efficiency from electric energy to chemical energy. Furthermore, the OER polarization curves of MFe-LDH (M= Ni, Co and Li) electrodeposited on glassy carbon (GC) electrode were studied (Fig. S8). The NiFe-LDH exhibits superior OER performances, with an onset potential of 1.43 V vs. RHE (the same value of Ni foam substrate) and an overpotential of 380 mV at a current density of 10 mA cm^{-2} (much lower than that of Ir/C (490 mV). It is worth mention that the current density of MFe-LDH nanoarrays supported on the Ni foam is larger than on the GC electrode at the same overpotential, which can be ascribed to the higher surface area of the Ni foam substrate.

To elucidate the intrinsic activities of MFe-LDH (M= Ni, Co and Li), density functional theory (DFT) calculations were carried out for the water oxidation reaction over these Fe-containing LDH samples (see computational details in the Supplementary Information). Generally, it has been proposed that electrocatalytic OER in alkaline media proceeds through multistep reactions:[50] (1) the formation of *OH intermediate from adsorbed H_2O on the active sites of catalyst; (2) a further oxidation or decomposition of *OH to *O; (3) the reaction of *O with H_2O molecule to produce *OOH intermediate; (4) the release of O_2 from *OOH. The OER performance correlates with the number of active sites and the adsorption affinity of H_2O and intermediates. The cumulative reaction free energies (ΔG_{298}) for the proposed reaction steps are plotted in Fig. S9. The binding energy of *O species (ΔG_{*O}) is larger than other species for all these three MFe-LDHs, indicating the oxidation of *O to *OOH is the rate-determining step. The ΔG_{*O} value increases as the following sequence: NiFe-LDH (1.506 eV) < CoFe-LDH (1.577 eV) < LiFe-LDH (1.653 eV). This yields overpotentials of 0.276 V, 0.347 V and 0.423 V for NiFe-, CoFe-, and LiFe-LDH, respectively, which is consistent with the order of experimental values. The results show NiFe-LDH gives the most thermodynamically favored reaction pathway (the lowest minimum overpotential), accounting for the best electrochemical performance in OER catalysis.

The OER performance of NiFe-LDH nanoplatelet arrays synthesized with different time was further studied. The corresponding LSV curves and Tafel plots are shown in Fig. S10. The overpotenial of NiFe-LDH firstly decreases gradually along with the increase of LDH deposition time and reaches a minimum for the NiFe-LDH (300 s) sample (Fig. 3d). However, the measured overpotenial both at 10 and 100 mA cm^{-2} increases significantly with further elongation of the deposition time. This result demonstrates that the coating of LDH at a suitable level can effectively enhance its OER activity; while an excess of LDH incorporation leads to a decreased catalytic efficiency, which may result from depressed active sites exposure and charge transfer (Fig. S4h-i). To further understand this trend, the electrochemical double layer capacitance was measured to determine the electrochemical surface area (ECSA) of NiFe-LDH samples with different mass loading (the linear slope of capacitive current vs. scan rate is equivalent to twice of the double layer capacitance C_{dl}[35]) (Fig. S11). It is found that the C_{dl} of NiFe-LDH firstly enhances gradually along with the increase of LDH deposition time and reaches a maximum for the NiFe-LDH (300 s) sample. However, the C_{dl} decreases significantly with further elongation of the deposition time. The results indicate that an excess of LDH loading leads to a decreased electrochemical surface area and the resulting depressed catalytic efficiency. Moreover, the electrochemical impedance spectroscopy (EIS) spectra for NiFe-LDH samples provide additional information about the charge transport properties (Fig. S12). The resistance increases slowly within the first 300 s, but enhances rapidly from 300 s to 500 s, indicating a depressed charge transport with dense loading of LDH. Therefore, the LDH nanoplatelets array grown on Ni foam with a suitable level would effectively enhance the OER activity;
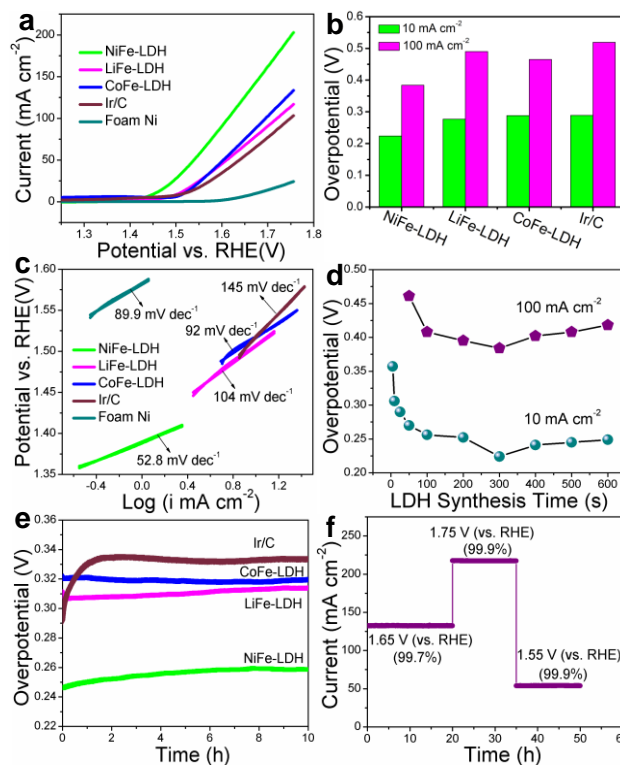
Fig. 3 (a) Linear sweep voltammetric (LSV) curves, (b) overpotential (at 10 and 100 mA cm^{-2}) and (c) Tafel plots of MFe-LDH (M= Ni, Co and Li) nanoplatelet arrays and commercial electrocatalyst Ir/C; (d) overpotential (at 10 and 100 mA cm^{-2}) of NiFe-LDH nanoplatelet arrays synthesized with various duration from 0 s to 600 s; (e) chronopotentiometric measurements at 10 mA cm^{-2} for MFe-LDH (M= Ni, Co and Li) nanoplatelet arrays and commercial Ir/C for 10 h; (f) chronoamperometric curve at varied overpotentials for NiFe-LDH nanoplatelet arrays.

while an excess of LDH loading leads to a decreased electrochemical surface area (ECSA) and depressed charge transport. A durability test of MFe-LDH nanoplatelet arrays was carried out by means of a chronopotentiometry measurement at 10 mA cm^{-2} (Fig. 3e). The operating overpotential for MFe-LDH (M= Ni, Co and Li) nanoplatelet arrays is nearly constant and only increases by 2%−5% after 10 h testing, indicating a good durability of MFe-LDH in alkaline solution. In contrast, the overpotential of the state-of-art OER catalyst Ir/C increases from 285 to 334 mV during only 2 h. Fig. 3f shows the current density curves as a function of time recorded at varied potentials for 50 h using NiFe-LDH electrode. It is found that the current density of OER remains constant at each given potentials (<1% current decay), further demonstrating the significantly long-term stability of NiFe-LDH electrocatalyst.

The OER performances of MFe-LDH synthesized by electrochemical method in this work are compared with other previously reported LDH-based eletrocatalysts (Table 1), which show obvious advantages. Firstly, previous LDHs-based electrodes normally require multi-steps, time- and energy-consuming procedures; while the electro-synthesized MFe-LDH can be obtained at room temperature within hundreds of seconds (<300 s). Secondly, the MFe-LDH nanoplatelet arrays with hierarchical architecture in this work guarantee a sufficient exposure of active sites and facilitate a fast mass/charge

Table 1. Comparison of synthesis method for Fe-containing LDHs and their OER activity in alkaline medium

Catalysts	Methods (Synthesis time)	Onset Potential (V vs. RHE)	η at J=10 mA cm^{-2} (mV)	J at η=300 mV (mA cm^{-2})	Stability	References
NiFe-LDH array	*In situ* growth (>24 h)	~1.46	~230	~40	10 h at 1.5V (~97%)	Ref. 38
Exfoliated NiFe-LDH nanosheet	Hydrothermal (>24 h)	~1.53	~290	~9	12 h at 10 mA cm^{-2} (~95%)	Ref. 37
NiFe-LDH particle	Hydrothermal (>24 h)	~1.43	~260	/	/	Ref. 45
NiFe-LDH array	electrosynthesis +aging (>24 h)	~1.46	/	/	12 h at 10 mA cm^{-2} (~99%)	Ref. 48
NiFe-LDH/Graphene particle	Hydrothermal (>24 h)	~1.44	~205	/	1.5 h at 5 mA cm^{-2} (~99%)	Ref. 39
NiFe-LDH/Graphene Ni foam	*In situ* growth (>24 h)	1.47	325	44	2.5 h at 10 mA cm^{-2} (~99%)	Ref. 40
nNiFe LDH/NGF	Hydrothermal (>24 h)	/	337	45	10 h at 1.58V (~99%)	Ref. 41
Ni$_{2/3}$Fe$_{1/3}$-rGO	Hydrothermal (>24 h)	/	~210	40	10 h at 10 mA cm^{-2} (~97%)	Ref. 42
NiFe-LDH/CQD particle	Hydrothermal (>24 h)	~1.46	235	~35	0.83 h at 2.5 mA cm^{-2} (~97%)	Ref. 43
NiFe-LDH/CNT particle	Hydrothermal (>24 h)	~1.45	~240	~45	0.28 h at 2.5 mA cm^{-2} (~100%)	Ref. 36
NiFe-LDH array	electro-synthesis (< 300 s)	~1.43	224	44	50 h at 1.55–1.75 V (~100%)	This work

transport, accounting for the largely-enhanced OER behavior. The onset potential and overpotential at 10 mA cm^{-2} of NiFe-LDH nanoplatelet arrays in this work are superior to previously reported NiFe-LDH based catalysts, such as pure LDH particles,[45] exfoliated NiFe-LDH nanosheets[37] as well as LDHs-based nanocomposites[39-43]. In addition, this electrosynthesized NiFe-LDH electrode is a carbon free system compared with most of the reported OER catalysts.

Electrochemical Oxidation of Hydrazine, Methanol and Ethanol

To validate the universal electrocatalytic activity of MFe-LDH nanoplatelet arrays, its catalytic performances toward electro-oxidation reactions of other small molecules was subsequently evaluated. The exploration of efficient catalysts for electro-oxidation of hydrazine is appealing because of its large hydrogen density delivery, high theoretical cell voltage and absence of CO$_2$ emission.[51-52] CVs and LSV curves of the MFe-LDH (M= Ni, Co and Li) nanoplatelet arrays, Ir/C and foam nickel substrate in 1 M KOH with 2 M hydrazine were measured. The oxidation current was normalized to the geometric surface areas; this allows the current density to be directly used to compare the catalytic activity of different samples. The CV curve of NiFe-LDH nanoplatelet arrays (Fig. 4a, inset) presents a significant negative-shift and anodic current increase with the addition of hydrazine, highlighting the remarkable electrocatalytic activity (onset potential ~0.2 V vs.

saturated calomel electrode, SCE). Furthermore, the LSV curves (Fig. 4a) of different MFe-LDH arrays and Ir/C catalyst in 1 M KOH solution with 2 M hydrazine demonstrate the electrocatalytic ability with the following sequence: NiFe-LDH > CoFe-LDH > LiFe-LDH ≥ Ir/C, which shows the same tendency of OER performance. The potentials at current density of 10 and 100 mA cm^{-2} for different catalysts are given in Fig. 4b. In the case of 100 mA cm^{-2}, the NiFe-LDH sample requires a potential of 244 mV, which is 85, 173, and 198 mV less than CoFe-LDH, LiFe-LDH and commercial Ir/C, respectively. It is worth mention that even with a low hydrazine concentration, a linear relationship between peak current over NiFe-LDH and hydrazine concentration in the range 2−20 mM is observed (Fig. 4c and Fig. S13), further demonstrating its remarkable catalytic activity.

To evaluate the electrocatalytic activity and stability of MFe-LDH under continuous operating conditions, long-term chronoamperometric tests at 10 mA cm^{-2} were carried out in a 1.0 M KOH + 2.0 M hydrazine solution (Fig. 4d). It is found that the required potential of NiFe-LDH at the same current density is smaller than that of CoFe-LDH, LiFe-LDH and Ir/C, highlighting a significantly improved electrocatalytic activity. Furthermore, NiFe-LDH nanoplatelet array catalyst exhibits largely enhanced long-term durability for hydrazine electro-oxidation. The electrochemical behavior of the MFe-LDH nanoplatelet arrays was further verified by the electrochemical
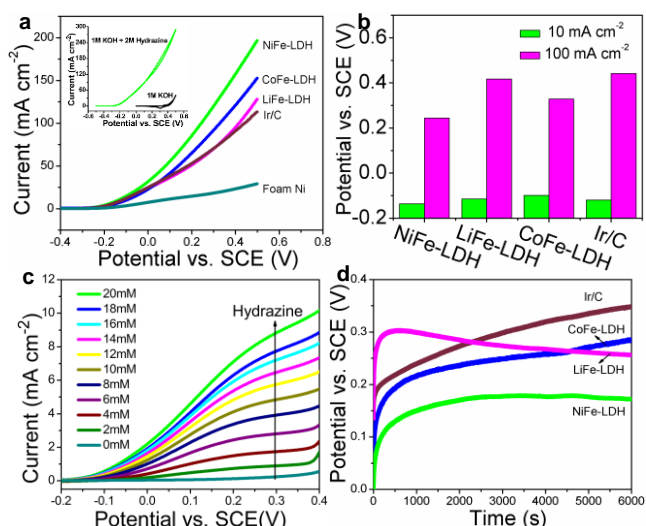
Fig. 4 (a) LSV curves of the MFe-LDH (M= Ni, Co and Li) nanoplatelet arrays, Ir/C and foam nickel substrate in 1 M KOH with 2 M hydrazine (inset: CVs of NiFe-LDH in 1 M KOH and 1 M KOH with 2 M hydrazine); scan rate: 0.1 V s^{-1}. (b) The required potentials of different electrocatalysts to reach current densities of 10 and 100 mA cm^{-2}. (c) LSV curves of the NiFe-LDH electrode in 1 M KOH solution with various concentrations of hydrazine; scan rate: 0.1 V s^{-1}. (d) Chronopotentiometric measurements at 10 mA cm^{-2} over MFe-LDH (M= Ni, Co and Li) nanoplatelet arrays and commercial Ir/C.

Fig. 5 (a) Photographs of NiFe-LDH nanoplatelet arrays synthesized on the foam nickel substrates with various scales (inset: the SEM image of NiFe-LDH on 100 cm^2 substrate); synthesis time for all the samples is 300 s at room temperature. SEM images for NiFe-LDH nanoplatelet arrays on (b) the conducting cloth and (c) FTO substrate (inset: their corresponding photographs).

oxidation of methanol and ethanol, which is estimable for low temperature direct fuel cell reactions. As shown in Fig. S14, the oxidation current is largely enhanced for the NiFe-LDH electrode with the presence of either methanol or ethanol. In addition, the sequence of electro-oxidation onset potential for the studied small molecules is as follows: hydrazine > water > methanol > ethanol. All the onset potentials for these molecules are relatively lower compared with previously reported values,[6,11,41] demonstrating a high activity of NiFe-LDH nanoarrays toward small molecules oxidation. This indicates that NiFe-LDH nanoarrays can be used as highly efficient electro-oxidation catalysts for energy conversion devices such as metal-air batteries and fuel cells.

Discussion

Although various LDHs-based materials have been investigated as OER catalysts and exhibited promising electrochemical properties, the majority of LDHs-based catalysts so far are difficult to be applied in practical applications due to their complicated preparation processing, high cost as well as uncontrollable nanostructures (e.g., particles have been mostly investigated, but suffer from aggregation). In this work, the hierarchical NiFe-LDH material demonstrates promising performances towards small molecules oxidation. This can be attributed to the ordered nanoplatelet array structure, which facilitates the electrolyte diffusion and electron transport. This is hardly achieved by random particles deposited on electrodes, as reported previously. Furthermore, the good chemical stability of LDHs in basic environment and the strong combination with the substrate extremely enhance the cycling stability of NiFe-LDH catalyst. As shown in Fig. S15, after 20 h and 5 h continuous OER and hydrazine oxidation testing, respectively,
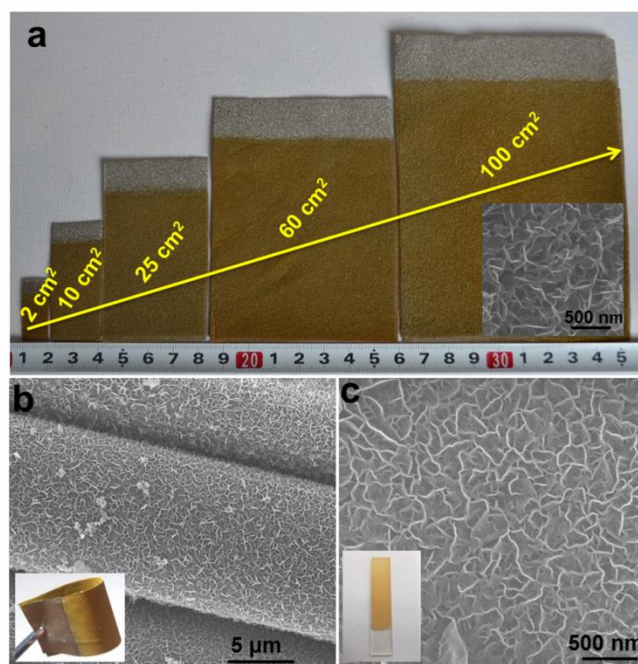
the surface of NiFe-LDH electrode maintains its original hierarchical array architecture. The high electro−oxidation catalytic activity along with the excellent cycling stability of MFe-LDHs meets the requirements of both high efficiency and long endurance simultaneously, which are prerequisites for practical applications. In addition, as shown in Fig. 5a, NiFe-LDHs nanoplatelet arrays directly growing on the foam nickel substrate can be effectively scaled up from 2 cm^2 to 100 cm^2 with uniform and homogeneous surface morphology. This electrosynthesis method is further adequate for the fabrication of NiFe-LDH nanoplatelet arrays on other conducting substrates, such as conducting clothes and glasses (Fig. 5b and 5c). The OER performances of NiFe-LDH arrays grown on Ni foam, conducting cloth and FTO were further studied. It is found that the NiFe-LDH/Ni foam displays the highest current density at the same overpotential (η) (Fig. S16), which can be ascribed to the large specific surface area and good conductivity of Ni foam. Therefore, the electrochemical preparation of MFe-LDHs array electrodes takes the advantages of simplicity, fast operation, low cost and high yield, which serves as a general strategy for the scalable manufacture of electrode materials. Besides the Fe-containing LDHs, this electrosynthesis method can be further extended for the preparation of LDHs nanoplatelet arrays with other compositions (e.g., Mn-containing LDHs, Co-containing LDHs) on the surface of various conducting substrates, which will be demonstrated in our near future work.

Conclusion

In summary, the hierarchical MFe-LDHs (M= Ni, Co and Li) nanoplatelet arrays have been successfully obtained via a fast and effective electrosynthesis method, which allows the crystallization of target materials in one synthetic step at room temperature. The obtained NiFe-LDH arrays display excellent catalytic activity and robust durability for small molecules electro-oxidation (H_2O and N_2H_4), superior to most of reported transition metal oxides/hydroxides catalysts as well as noble metal catalysts such as Ir/C (20 wt%). Considering the catalytic capability toward oxidation reaction of small fuel molecules, Fe-containing LDHs electrodes fabricated by electrosynthesis method are promising for direct use in water-splitting devices and fuel cells. Moreover, we believe that the reported synthetic approach can be further extended to other types of LDHs-based nanostructures for advanced performances in the fields of energy conversion and storage.

Acknowledgements

Notes and references

1   W. Tang, Y. Han, C. B. Han, C. Z. Gao, X. Cao, Z. L. Wang, *Adv. Mater.*, 2015, **27**, 272.
2   J. N. Tiwari, R. N. Tiwari, G. Singh, K. S. Kim, *Nano Energy*, 2013, **2**, 553.
3   A. Serov, M. Padilla, A. J. Roy, P. Atanassov, T. Sakamoto, K. Asazawa, H. Tanaka, *Angew. Chem. Int. Ed.*, 2014, **39**, 10504.
4   L. G. Feng, K. Li, J. F. Chang, C. P. Liu, W. Xing, *Nano Energy*, 2015, **15**, 462.
5   R. Subbaraman, D. Tripkovic, K. C. Chang, D. Strmcnik, A. P. Paulikas, P. Hirunsit, M. Chan, J. Greeley, V. Stamenkovic, N. M. Markovic, *Nat. Mater.*, 2012, **11**, 550.
6   R. L. Liu, F. L. Liang, W. Zhou, Y. S. Yang, Z. H. Zhu, *Nano Energy*, 2015, **12**, 115.
7   Y. Liang, Y. Li, H. Wang, H. J. Dai, *J. Am. Chem. Soc.*, 2013, **135**, 2013.
8   S. Ci, S. Mao, Y. Hou, S. Cui, H. Kim, R. Ren, Z. Wen, J. Chen, *J. Mater. Chem. A*, 2015, **3**, 7986.
9   X. Cao, N. Wang, Y. Han, C. Gao, Y. Xu, M. Li, Y. H. Shao, *Nano Energy*, 2015, **12**, 105.
10 M. K. Debe, *Nature*, 2012, **486**, 43.
11 P. Kannan, T. Maiyalagan, M. Opallo, *Nano Energy*, 2013, **2**, 677.
12 C. Bianchini, P. K. Shen, *Chem. Rev.*, 2009, **109**, 4183.
13 M. Liu, Y. Lu, W. Chen, *Adv. Funct. Mater.*, 2013, **23**, 1289.
14 M. G. Walter, E. L. Warren, J. R. Mckone, S. W. Boettcher, Q. Mi, E. A. Santori, N. S. Lewis, *Chem. Rev.*, 2010, **110**, 6446.
15 Y. Lee, J. Suntivich, K. J. May, E. E. Perry, Y. Shao-Horn, *J. Phys. Chem. Lett.*, 2012, **3**, 399.
16 Z. Zhuang, W. Sheng, Y. Yan, *Adv. Mater.*, 2014, **26**, 3950.
17 R. Chen. H-Y. Wang, J. Miao, H. Yang, B. Liu, *Nano Energy*, 2015, **11**, 333.
18 M. Barroso, A. J. Cowan, S. R. Pendlebury, M. Gratzel, D. R. Klug, J. R. Durrant, *J. Am. Chem. Soc.*, 2011, **133**, 14868.
19 B. Ni, X. Wang, *Chem. Sci.*, 2015, **6**, 3572.
20 J. Suntivich, K. J. May, H. A. Gasteiger, J. B. Goodenough, Y. Shao-Horn, *Science*, 2011, **334**, 1383.
21 R. N. Singh, T. Sharma, A. Singha, D. Mishra, S. K. Tiwari, *Electrochim. Acta.*, 2008, **53**, 2322.
22 H. W. Park, D. U. Lee, P. Zamani, M. H. Seo, L. F. Nazar, Z. W. Chen, *Nano Energy*, 2014, **10**, 192.
23 W. D. Chemelewski, H. C. Lee, J. F. Lin, A. J. Bard, C. B. Mullins, *J. Am. Chem. Soc.*, 2014, **136**, 2843.
24 R. L. Spray, K. S. Choi, *Chem. Mater.*, 2009, **21**, 3701.
25 Y. Miao, L. Ouyang, S. Zhou, L. Xu, Z. Yang, M. Xiao, R. Ouyang, *Biosens. Bioelectron.*, 2014, **53**, 428.
26 Q. Wang, D. O'Hare, *Chem. Rev.*, 2012, **112**, 4124.
27 M. Shao, F. Ning, J. Zhao, M. Wei, D. G. Evans, X. Duan, *J. Am. Chem. Soc.*, 2012, **134**, 1071.
28 J. K. Gunjakar, T. W. Kim, H. N. Kim, I. Y. Kim, S. J. Hwang, *J. Am. Chem. Soc.*, 2011, **133**, 14998.
29 M. Q. Zhao, Q. Zhang, J. Q. Huang, G. L. Tian, J. Q. Nie, H. J. Peng, F. Wei, *Nat. Commun.*, 2014, **5**, 3410.
30 M. Q. Zhao, Q. Zhang, W. Zhang, J. Q. Huang, Y. Zhang, D. S. Su, F. Wei, *J. Am. Chem. Soc.*, 2010, **132**, 14739.
31 C. Chen, M. Yang, Q. Wang, J. C. Buffet, D. O'Hare, *J. Mater. Chem. A*, 2014, **2**, 15102.
32 Y. Zhang, B. Cui, C. Zhao, H. Lin, *Phys. Chem. Chem. Phys.*, 2013, **15**, 7363.
33 F. Song, X. Hu, *J. Am. Chem. Soc.*, 2014, **136**, 16481.
34 Y. Zhao, B. Li, Q. Wang, W. Gao, C. J. Wang, M. Wei, D. G. Evans, X. Duan, D. O'Hare, *Chem. Sci.*, 2014, **5**, 951.
35 X. Zou, A. Goswami, T. Asefa, *J. Am. Chem. Soc.*, 2013, **135**, 17242.
36 M. Gong, Y. Li, H. Wang, Y. Liang, J. Z. Wu, J. Zhou, J. Wang, T. Regier, F. Wei, H. J. Dai, *J. Am. Chem. Soc.*, 2013, **135**, 8452.
37 F. Song, X. Hu, *Nat. Commun.*, 2014, **5**, 4477.
38 Z. Lu, W. Xu, W. Zhu, X. Sun, X. Duan, *Chem. Commun.*, 2014, **50**, 6479.
39 X. Long, J. Li, S. Xiao, K. Yan, Z. Wang, H. Chen, S. Yang, *Angew. Chem. Int. Ed.*, 2014, **53**, 7584.
40 H. F. Wang, C. Tang, Q. Zhang, *J. Mater. Chem. A*, 2015, **3**, 16183.
41 C. Tang, H. Wang, H. Wang, Q. Zhang, G. Tian, J. Nie, F. Wei, *Adv. Mater.*, 2015, DOI: 10.1002/adma.201501901.
42 W. Ma, R. Ma, C. Wang, J. Liang, X. Liu, K. Zhou, T. Sasaki, *ACS Nano*, 2015, **9**, 1977.
43 D. Tang, J. Liu, X. Wu, R. Liu, X. Han, Y. Han, H. Huang, Y. Liu, Z. Kang, *ACS. Appl.Mater. Inerfaces.*, 2014, **6**, 7918.
44 X. Long, S. Xiao, Z. Wang, X. Zheng, S. Yang, *Chem. Commun.*, 2015, **51**, 1120.
45 B. Hunter, J. Blakemore, M. Deimund, H. Gray, J. Winkler, *J. Am. Chem. Soc.*, 2014, **136**, 13118.
46 D. A. Corrigan, *J. Electrochem. Soc.*, 1987, **134**, 377.
47 D. A. Corrigan, R. M. Bendert, *J. Electrochem. Soc.*, 1989, **136**, 723.
48 L. Trotochaud, S. Young, J. Ranney, S. Boettcher, *J. Am. Chem. Soc.*, **136**, 6744.
49 T. Yamashita, P. Hayes, *Appl. Surf. Sci.*, 2008, **254**, 2441.
50 D. Friebel, M. W. Louie, M. Bajdich, K. E. Sanwald, Y. Cai, A. M. Wise, M. J. Cheng, D. Sokaras, T. C. Weng, R. Alonso-Mori, R. C. Davis, J. R. Bargar, J. K. Nørskov, A. Nilsson, A. T. Bell, *J. Am. Chem. Soc.*, 2015, **137**, 1305.
51 N. V. Rees, R. G. Compton, *Energy Environ. Sci.*, 2011, **4**, 1255.
52 L. Aldous, R. G. Compton, *Phys. Chem. Chem. Phys.*, 2011, **13**, 5279.